Supporting Information

Spatially Resolving the Enhancement Effect in Surface-Enhanced Coherent Anti-Stokes Raman Scattering by Plasmonic Doppler Gratings

Lei Ouyang[†,‡,§] Tobias Meyer[†,‡], Kel-Meng See[⊥], Wei-Liang Chen[‖], Fan-Cheng Lin[⊥], Denis Akimov[†,‡], Sadaf Ehtesabi[‡], Martin Richter[‡], Michael Schmitt[†,‡], Yu-Ming Chang[‖], Stefanie Gräfe[‡], Jürgen Popp[†,‡], Jer-Shing Huang[†,‡,⊥,#,Δ,*]

[†] Leibniz Institute of Photonic Technology, Albert-Einstein Str. 9, 07745 Jena, Germany
[‡] Institute of Physical Chemistry and Abbe Center of Photonics, Friedrich-Schiller-Universität Jena, Helmholtzweg 4, D-07743 Jena, Germany
[§] School of Chemistry and Chemical Engineering, Huazhong University of Science and Technology, Wuhan 430074, China
[⊥] Department of Chemistry, National Tsing Hua University, 101 Sec. 2, Kuang-Fu Road, Hsinchu 30013, Taiwan
[‖] Center for Condensed Matter Sciences, National Taiwan University, Taipei 10617, Taiwan
[#] Research Center for Applied Sciences, Academia Sinica, 128 Sec. 2, Academia Road, Nankang District, Taipei 11529, Taiwan
[Δ] Department of Electrophysics, National Chiao Tung University, Hsinchu 30010, Taiwan
*Corresponding Author, E-mail: jer-shing.huang@leibniz-ipht.de

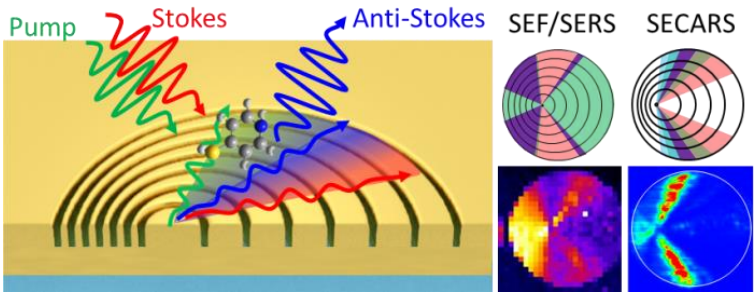

Content:

I. DFT calculation (Figure S1)
II. Experimental setup (Figure S2)
III. Video of SERS image evolution (video for PDG-SERS.mp4)
IV. FDTD simulations (Figures S3 and S4)
V. Pixel-to-azimuthal angle conversion (Figure S5)

I. DFT calculation

In this section, we show by Density Functional Theory (DFT) calculations that the characteristic Raman peak used in this work (1070 cm^{-1}) is significantly enhanced by the binding of the 4-Aminothiophenol (4-ATP) molecule to the Au surface. All geometry optimizations, including the cases of isolated 4-ATP (Figure S1a) and 4-ATP attached to the Au surface in 3 different possible orientations (Figure. S1b-S1d), were done using DFT as implemented in GPAW code[1,2] with ASE[3] interface. For this purpose, the optB88-vdW functional[4] is employed in a real-space grid.

The Au slab is represented by a 4×4×3 fcc(111) surface, resulting in 3 layers of 16 Au atoms with two-dimensional periodic boundary conditions (x and y directions). 4-ATP molecules bind strongly to the Au surface through the Au-S bond. To reduce the computational cost of the geometry optimizations, the second and third layer of the Au slab were fixed, and only the geometry of the molecule and Au atoms in the first layer were optimized.

We simulated 3 representative orientations of the 4-ATP molecule with respect to the surface. The first orientation is shown in the inset of Figure S1b, where the molecule binds to the surface through the S atom, and the plane of the phenyl ring is perpendicular to the Au surface. We call this configuration "structure 1". The second orientation is shown in the inset of Figure S1c, where the molecule binds to the surface through the S and H atom. The plane of the phenyl ring is still perpendicular to the Au surface. This configuration is called "structure 2". The third orientation is a "flat-lying" configuration as shown in the insets of Figure S1d. In this configuration, the phenyl ring is parallel to the gold surface. Therefore, the molecule binds to the surface through the interaction of the gold surface with the S atom and with the π orbitals of the phenyl ring. We call this configuration "structure 3".

To obtain the Raman spectra, the vibrational frequencies were calculated using DFT employing the CAM-B3LYP[5] functional and def2-tzvp basis set using Gaussian 09.[6] The frequencies were scaled by a factor of 0.95 to correct for the lack of anharmonicity and the approximate treatment of electron correlation.[7] All vibrational frequency calculations were performed including D3 dispersion correction with Becke-Johnson damping.[8] Figure S1a shows the calculated Raman spectrum of an isolated 4-ATP molecule. Figures S1b to S1d show the calculated spectra of the corresponding configuration shown in their insets. By comparing Figure S1a with Figure. S1b and S1c, it is clear that the characteristic Raman peak at 1070 cm^{-1}, which stems from the vibration of the phenyl ring is significantly enhanced by

binding of the 4-ATP molecule to the Au surface. By comparing Figure. S1b and S1c with S1d, it is further obvious that 4-ATP molecules with a perpendicular orientation with respect to the Au surface (structure 1 and structure 2) show an approximately three orders of magnitude stronger Raman signal at 1070 cm^{-1} than that of a flat-lying molecule (structure 3). Figure S1e compares the Raman spectra shown in Figure. S1a to S1d. Apparently, attaching the 4-ATP to the gold surface greatly enhances the 1070 cm^{-1} Raman peak, standing out from the background. Therefore, this peak has been chosen as a targeted peak in our SECARS experiment.

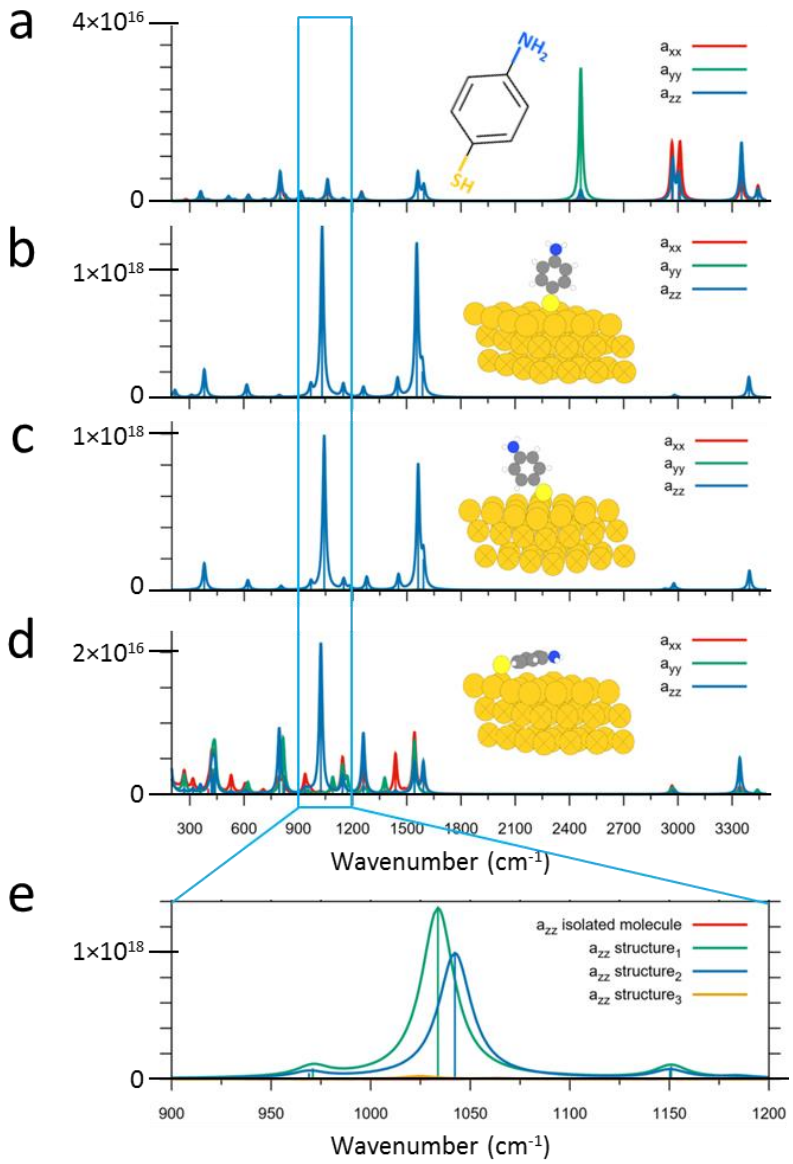

Figure S1. (a) Calculated Raman spectrum of an isolated 4-ATP molecule. (b) Calculated Raman spectrum of "structure 1" configuration in the inset. (c) Raman spectrum of "structure 2" configuration in the inset. (d) Raman spectrum of "structure 3" configuration in the inset. Legends in (a) to (d) indicate the different components of the polarizability tensor α, where the coordinate system is such defined that the z-direction points normal to the gold surface. (e) The 1070 cm^{-1} peak of isolated 4-ATP and 4-ATP attached to the Au surface in different orientations.

II. Experimental setup

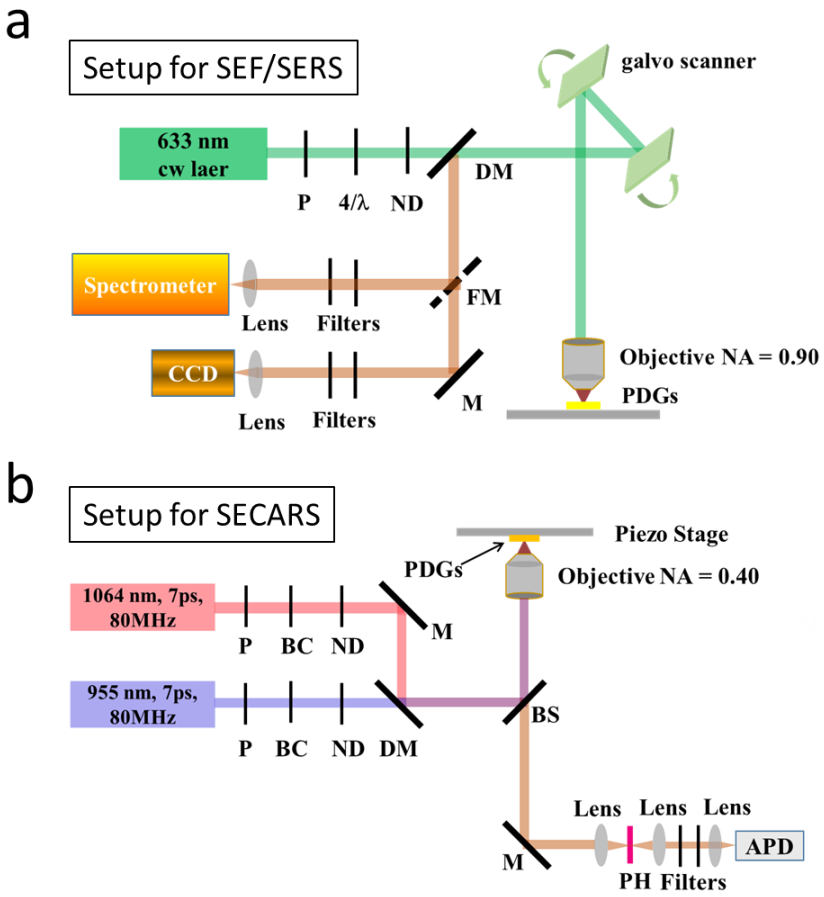

Figure S2. (a) The setup for SERS mapping. P: polarizer, 4/λ: quarter wave-plate, ND: neutral density filter, M: mirror, DM: dichroic mirror, FM: flip mirror. (b) The setup for SECARS intensity mapping. P: polarizer, BC: Berek compensator, ND: neutral density filter, M: mirror, DM: dichroic mirror, BS: 50/50 beam splitter, FM: flip mirror, PH: pinhole.

III. Video of SERS image evolution

"video for PDG-SERS.mp4"

The movie shows the evolution of the SEF/SERS map as the Stokes shift is scanned from 400 to 2650 cm^{-1}, corresponding to the spectrum and images shown in Figures 3d and 3e, respectively, in the main text.

IV. FDTD simulations

a. Enhancement in the input beams (pump and Stokes)

Planewave source was used to illuminate onto the structure with incident angle increasing from 0 to 23.6°, corresponding to the allowed angle provided by a NA 0.4 objective. The grating period was scanned from 300 to 1100 nm, three point-monitors were placed at three representative positions, which are 5 nm above the structure surface, as shown in Figure S3a. The electric field (E^2) intensity recorded by the point monitors was then divided by E_0^2 to obtain the enhancement factor. The E_0^2 is the electric field recorded by a point monitor placed 5 nm above a flat Au surface. The enhancement factors at the three locations were then used to calculate the averaged enhancement factor for the molecular monolayer covering the surface of the grating. The averaged enhancement factor is calculated area using the formula $\left(\frac{E^2}{E_0^2}\right)_{\text{average}} = \frac{\frac{1}{2}\left(\frac{E_1^2}{E_0^2}+\frac{E_3^2}{E_0^2}\right)*groove\ area + \frac{1}{2}\left(\frac{E_1^2}{E_0^2}+\frac{E_2^2}{E_0^2}\right)*flat\ area}{groove\ area + flat\ area}$.

Taking the dimensions of the structure estimated according to the SEM image (bottom panel of Figure S3a), the formula becomes $\left(\frac{E^2}{E_0^2}\right)_{\text{average}} = \frac{\frac{1}{2}\left(\frac{E_1^2}{E_0^2}+\frac{E_3^2}{E_0^2}\right)*2*\sqrt{(35^2+140^2)} + \frac{1}{2}\left(\frac{E_1^2}{E_0^2}+\frac{E_2^2}{E_0^2}\right)*(P-70)}{2*\sqrt{(35^2+140^2)}+(P-70)}$.

The averaged enhancement was replotted *versus* the azimuthal angle and incident angle for the pump and Stokes beams in Figure. S3b and S3c, respectively. The enhancement factor at a specific azimuthal angle is obtained by averaging the enhancement factor of all possible incident angles. This results in the angle profiles for pump and Stokes shown in Figure 4(c) in the main text.

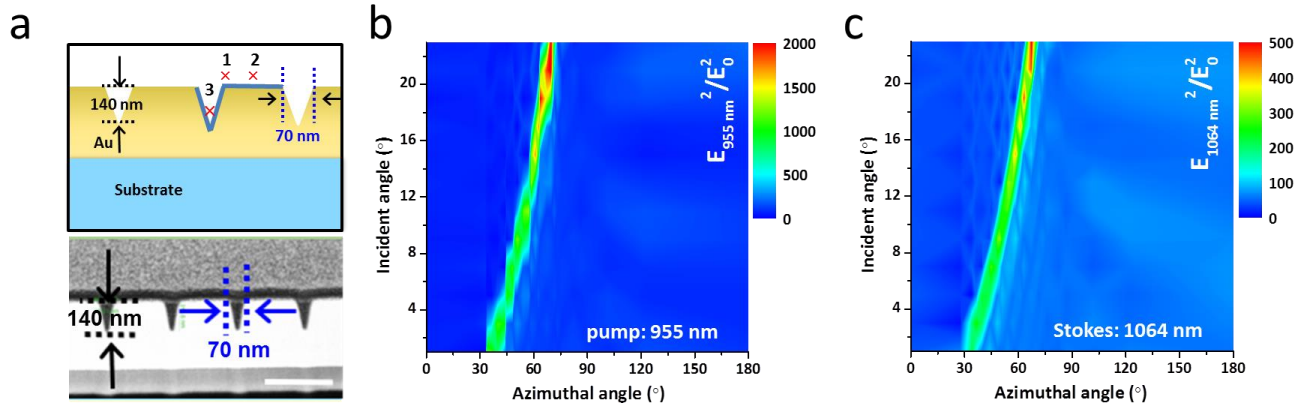

Figure S3. (a) Top panel: the grating structure used in the FDTD simulations. The three point-monitors were placed 5 nm above the gold surface at the positions marked by red crosses with a number. Bottom panel: the cross-sectional TEM image of the real structure. The gap width and depth are estimated to be around 70 nm and 140 nm, respectively. (b) and (c): The averaged enhancement factor for the pump and Stokes beam at 955 nm and 1064 nm, respectively, on the 2D plane of the incident and azimuthal angle. Scale bar = 500 nm.

b. Enhancement in the output beam (anti-Stokes)

A dipole source was placed 5 nm above the structure at three different locations (Figure S4a). The polarization of the dipole source is in-plane along the x-axis, *i.e.*, perpendicular to the grating grooves. A line monitor was placed 20 nm above the upper surface of the structure. The grating period was scanned from 300 to 1100 nm. The far-field projection of the electric field intensity recorded at 867 nm (anti-Stokes) by the line monitor allows for the calculation of the emission power as a function of the emitting angle. The azimuthal and emission angle-dependent electric field intensity with a single dipole source placed at three representative positions is shown in Figure S4b. The collectible emitted electric field intensity (E^2) at a specific azimuthal angle (*i.e.* a specific grating periodicity) is obtained by summing up the electric field intensity for all allowed emission angles defined by the numerical aperture of the objective (NA = 0.4), *i.e.*, the angle between ± 23.6˚. Enhancement E^2/E_0^2 was calculated by dividing the E^2 with E_0^2, where E_0^2 is the emitted power obtained with a dipole source on a flat gold surface. The area-averaged enhancement factor was calculated in a way similar to the calculation for the enhancement in the input beams. The area-averaged enhancement plotted *versus* the azimuthal and emission angle is shown in Figure S4b. The enhancement factor at a specific azimuthal angle is obtained by summing up the enhancement factor for all allowed emission angles within the numerical aperture of the objective (NA = 0.4), *i.e.*, all angles between ± 23.6˚. This produces the enhancement angle profiles for the anti-Stokes beam shown in Figure 4(c) in the main text.

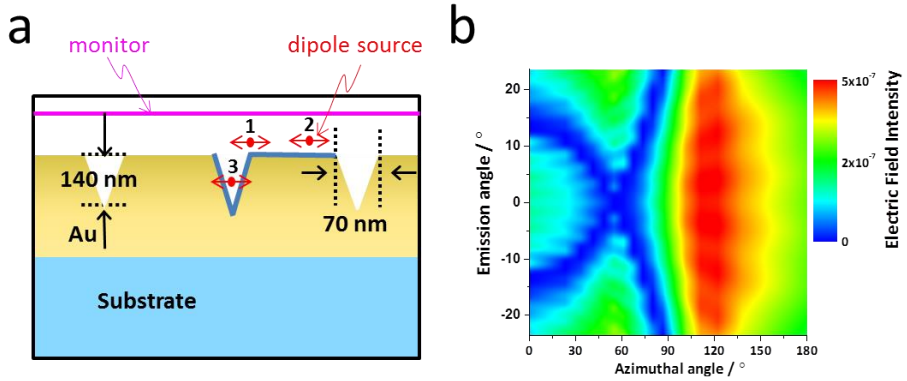

Figure S4. (a) The grating structure for simulating the output enhancement of the anti-Stokes beam (867 nm). Three double arrows indicate the three representative positions and orientation of a single dipole source on the grating. A line monitor (magenta line) was placed 20 nm above the upper surface of the structure to record the emission power from the dipole source. (b) The azimuthal angle and emission angle-dependent electric field intensity distribution for anti-Stokes output at 867 nm with the dipole placed at point 2.

V. Pixel-to-azimuthal angle conversion

To directly compare the angle distribution of the experimental SECARS intensity with the simulated enhancement, the coordinate of each intensity pixel in the intensity map (Figure 4a in the main text) was transformed into the azimuthal angle (φ) with respect to the center of the PDG, *i.e.*, the position of the smallest ring with a zero radius (x_0, y_0) using $\varphi = \operatorname{actan}\frac{|y_n - y_0|}{|x_n - x_0|}$. Figure S5 illustrates the pixel-to-azimuthal angle conversion.

The calculated azimuthal angle for each pixel was rounded to the nearest integer of one degree. Intensities of all pixels within the bandwidth of one degree were summed up and divided by the pixel number to obtain the averaged intensity, as shown by the red trace in Figure 4d in the main text.

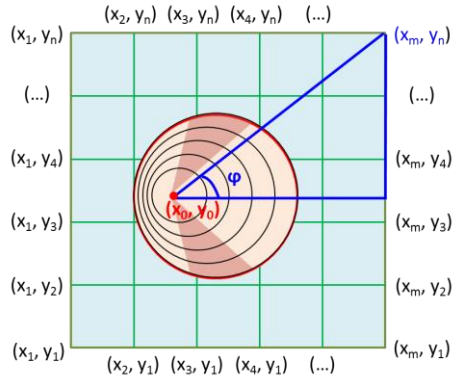

Figure S5. Schematic illustration of the pixel-to-azimuthal angle conversion. For the clarity of illustration, the size of pixels has been enlarged.

REFERENCES

1. Mortensen, J. J.; Hansen, L. B.; Jacobsen, K. W., Real-Space Grid Implementation of the Projector Augmented Wave Method. *Phys. Rev. B* **2005,** 71, 035109.
2. Enkovaara, J.; Rostgaard, C.; Mortensen, J. J.; Chen, J.; Dulak, M.; Ferrighi, L.; Gavnholt, J.; Glinsvad, C.; Haikola, V.; Hansen, H. A.; Kritstoffersen, H. H.; Kuisma, M.; Larsen, A. H.; Lehtovaara, L.; Ljungberg, M.; Lopez-Acevedo, O.; Moses, P. G.; Ojanen, J.; Olsen, T.; Petzold, V., *et al*., Electronic Structure Calculations with GPAW: A Real-Space Implementation of the Projector Augmented-Wave Method. *J. Phys.: Condens. Matter* **2010,** 22, 253202.
3. Larsen, A. H.; Mortensen, J. J.; Blomqvist, J.; Castelli, I. E.; Christensen, R.; Dulak, M.; Friis, J.; Groves, M. N.; Hammer, B.; Hargus, C.; Hermes, E. D.; Jennings, P. C.; Jensen, P. B.; Kermode, J.; Kitchin, J. R.; Kolsbjerg, E. L.; Kubal, J.; Kaasbjerg, K.; Lysgaard, S.; Moronsson, J. B., *et al.*, The Atomic Simulation Environment - A Python Library for Working with Atoms. *J. Phys.: Condens. Matter* **2017**, 29, 273002.
4. Klimeš, J.; Bowler, D. R.; Michaelides, A, Chemical Accuracy for the van der Waals Density Functional. *J. Phys.: Conden. Matter* **2010**, 22, 022201.
5. Yanai, T.; Tew, D. P.; Handy, N. C., A New Hybrid Exchange–Correlation Functional Using the Coulombattenuating Method (CAM-B3LYP). *Chem. Phys. Lett.* **2004**, 393, 51–57.
6. Frisch, M. J.; Trucks, G. W.; Schlegel, H. B., Scuseria, G. E.; Robb, M. A.; Cheeseman, J. R.; Scalmani, G.; Barone, V.; Mennucci, B.; Petersson, G. A.; Nakatsuji, H.; Caricato, M.; Li, X.; Hratchian, H. P.; Izmaylov, A. F.; Bloino, J.; Zheng, G.; Sonnenberg, J. L.; Hada, M.; Ehara, M., *et al.*, Gaussian 09, Revision A.1, Gaussian, Inc., Wallingford, CT, **2009**.
7. Merrick, J. P.; Moran, D.; Radom, L., An Evaluation of Harmonic Vibrational Frequency Scale Factors. *J. Phys. Chem.* **2007**, 111, 11683–11700.
8. Grimme, S.; Ehrlich, S.; Goerigk, L., Effect of the Damping Function in Dispersion Corrected Density Functional Theory. *J. Comput. Chem*. **2011**, 32, 1456–1465.